Electronic and Optical Excitations in van der Waals Materials from a Non-Empirical Wannier-Localized Optimally-Tuned Screened Range-Separated Hybrid Functional

María Camarasa-Gómez,[1,*] Stephen E. Gant,[2,3] Guy Ohad,[1] Jeffrey B. Neaton,[2,3,4] Ashwin Ramasubramaniam,[5,6,†] and Leeor Kronik[1,‡]

[1] *Department of Molecular Chemistry and Materials Science, Weizmann Institute of Science, Rehovoth 7610001, Israel*
[2] *Department of Physics, University of California, Berkeley, CA 94720, USA*
[3] *Materials Sciences Division, Lawrence Berkeley National Laboratory, Berkeley, CA 94720, USA*
[4] *Kavli Energy NanoSciences Institute at Berkeley, University of California, Berkeley, CA 94720, USA*
[5] *Department of Mechanical and Industrial Engineering, University of Massachusetts Amherst, Amherst MA 01003, USA*
[6] *Materials Science and Engineering Graduate Program, University of Massachusetts, Amherst, Amherst MA 01003, USA*

(Dated: May 2, 2024)

Accurate prediction of electronic and optical excitations in van der Waals (vdW) materials is a long-standing challenge for density functional theory. The recently proposed Wannier-localized optimally-tuned screened range-separated hybrid (WOT-SRSH) functional has proven successful in non-empirical determination of electronic band gaps and optical absorption spectra for various covalent and ionic crystals. However, for vdW materials the tuning of the material- and structure-dependent functional parameters has, until now, only been attained semi-empirically. Here, we present a non-empirical WOT-SRSH approach applicable to vdW materials, with the optimal functional parameters transferable between monolayer and bulk. We apply this methodology to prototypical vdW materials: black phosphrous, moldybdenum disulfide, and hexagonal boron nitride (in the latter case including zero-point renormalization). We show that the WOT-SRSH approach consistently achieves accuracy levels comparable to experiments and *ab initio* many-body perturbation theory (MBPT) calculations for band structures and optical absorption spectra, both on its own and as an optimal starting point for MBPT calculations.

Van der Waals (vdW) materials [1–7], comprised of weakly interacting stacks of (quasi-)two-dimensional (2D) layers, have attracted much interest owing to the outstanding tunability of their electronic and optical properties with the number, composition, and orientation of individual 2D layers. The unique properties of these materials have also motivated an ongoing effort in accurate prediction of their electronic band structures and optical absorption spectra [8, 9]. Often this is based on *ab initio* many-body perturbation theory (MBPT) [10, 11] within the framework of the GW method [12] and the Bethe-Salpeter equation (BSE) [13, 14]. However, there is significant interest in more readily affordable computational approaches rooted in density functional theory (DFT) [15, 16]. Recent methodological developments within DFT have greatly improved the quantitative accuracy of band gap predictions in solids. Notable examples are Koopmans-compliant functionals [17–22], localized orbital scaling corrections [23–25], dielectric-dependent functionals [26–31], and screened range-separated hybrid (SRSH) functionals [32–37].

Here, we focus on a recently introduced specific class of SRSH functionals, Wannier-localized optimally-tuned (WOT)-SRSH functionals [37–40], because they combine three advantages: They are non-empirical, with physical parameters derived directly from the pristine system [37]; They can be applied to both molecules [41] and solids [37]; They lend themselves naturally to computation of optical absorption directly from time-dependent (TD) DFT [33, 40, 42].

In the SRSH approach, correct asymptotic dielectric screening is introduced via screened long-range exchange, while short-range exchange provides a good balance with dynamic correlation and mitigates self-interaction errors [32, 42, 43]. The transition between short- and long-range exchange is governed by a range-separation parameter. For bulk solids, the fraction of short-range exchange and the range-separation parameter have been successfully determined non-empirically via the Wannier-localized optimal tuning procedure [37], elaborated below. For vdW materials, however, the need to address both monolayer and bulk with a consistent set of parameters has to date hindered use of the WOT approach. In prior work, the requisite SRSH parameters were determined semi-empirically by fitting to MBPT-computed gaps [44, 45], thereby strongly limiting the predictive power of the method for this important class of materials.

In this article, we obtain non-empirical SRSH functionals suitable for vdW materials, entirely from first principles, via a generalized WOT procedure. Specifically, we

* maria.camarasa-gomez@weizmann.ac.il
† ashwin@umass.edu
‡ leeor.kronik@weizmann.ac.il

present an internally self-consistent framework that exploits an ionization potential (IP) ansatz [17, 37] to determine optimal parameters of a fully non-empirical SRSH, for both monolayer and bulk phases of any specific vdW material. We apply this approach to three representative vdW materials – black phosphorus (bP), molybdenum disulfide (MoS_2), and hexagonal-boron nitride (h-BN) – that are prototypical examples of narrow, moderate, and wide gap semiconductors, respectively. Our calculated electronic bandstructures and optical absorption spectra are in excellent agreement with both experimental and MBPT studies for all materials. Even the gap of monolayer h-BN, which has previously been shown to be challenging for SRSH functionals [44], is now predicted correctly once zero-point renormalization (ZPR) of the electronic band gap is properly taken into account. This confirms the accuracy of the self-consistent tuning approach and opens the door to truly predictive use of WOT-SRSH functionals in, e.g., high-throughput screening and design of vdW materials [46, 47].

The SRSH functional is based on a decomposition of the Coulomb interaction, $1/r$ [48], in the form [49]

$$\frac{1}{r} = \frac{\alpha + \beta\,\mathrm{erf}(\gamma r)}{r} + \frac{1 - [\alpha + \beta\,\mathrm{erf}(\gamma r)]}{r}, \qquad (1)$$

where $\mathrm{erf}(\cdot)$ is the error function and α, β, γ are parameters. The first term of Eq. (1) is treated using exact (Fock) exchange (XX) whereas the second term is treated using semilocal (SL) DFT exchange. This naturally partitions the exchange interaction into short-range (SR) and long-range (LR) components, where the XX fraction is α in the SR and $\alpha + \beta$ in the LR (with complementary SL exchange, SLx, fractions), and γ is the range-separation parameter.

To enforce asymptotic screening of the Coulomb repulsion in a three-dimensional (3D) solid (neglecting anisotropy), we set $\alpha + \beta$ to $1/\epsilon_\infty$, the high-frequency scalar dielectric constant (obtained as the average of the diagonal terms of the dielectric tensor) [32, 50]. The corresponding non-multiplicative exchange potential, v_x^{SRSH}, obtained within generalized Kohn-Sham theory [51–55], is then given by

$$v_x^{\mathrm{SRSH}} = \alpha v_{\mathrm{XX}}^{\mathrm{SR}} + (1-\alpha) v_{\mathrm{SLx}}^{\mathrm{SR}} + \frac{1}{\epsilon_\infty} v_{\mathrm{XX}}^{\mathrm{LR}} + \left(1 - \frac{1}{\epsilon_\infty}\right) v_{\mathrm{SLx}}^{\mathrm{LR}}. \qquad (2)$$

For 2D solids, we set $\epsilon_\infty = 1$, as this is the formal exact asymptotic limit for screening in 2D materials [56–58]. While this is the correct asymptotic limit in all three directions, anisotropy in the division between short range and long range is still not accounted for explicitly, but we show below that this is already sufficient for obtaining excellent results nonetheless.

While ϵ_∞ can be calculated routinely from first principles [59, 60], α and γ must be determined by other means. Previously, this has only been accomplished by simultaneous fitting to benchmark band gaps of monolayer and bulk phases [44, 45], an approach denoted henceforth as semi-empirical (SE) SRSH. Here, we move beyond it by generalizing the non-empirical WOT scheme,[37–40] previously used in 3D solids. WOT enforces the IP ansatz for removal of charge from the maximally localized Wannier function, ϕ, with the highest one-electron expectation energy, such that for any given value of α we seek γ that obeys

$$\Delta I^\gamma = E^\gamma_{\mathrm{constr}}[\phi](N-1) - E^\gamma(N) + \langle\phi|\,\hat{H}^\gamma_{\mathrm{SRSH}}\,|\phi\rangle = 0, \qquad (3)$$

where $E^\gamma(N)$ is the total energy of the neutral N-electron system, $E^\gamma_{\mathrm{constr}}[\phi](N-1)$ is the total energy (calculated via a constrained minimization procedure [37]) of the system with one electron subtracted from ϕ, and $\langle\phi|\,\hat{H}^\gamma_{\mathrm{SRSH}}\,|\phi\rangle$ is the expectation value of the SRSH Hamiltonian, $\hat{H}^\gamma_{\mathrm{SRSH}}$, with respect to the Wannier function. An example of ϕ, for h-BN, is given in Fig. 1(a) [Section I of the Supporting Information (SI) contains the equivalent of Fig. 1 for black phosphorus (bP) and molybdenum disulfide (MoS_2)].

The above-explained WOT procedure is demonstrated in Fig. 1(b), which shows $\Delta I(\gamma)$ curves for various values of α, for both bulk (3D ϵ_∞) and monolayer ($\epsilon_\infty = 1$). The Figure shows that even over the relatively limited range of α and γ values depicted, the bulk band gap can change by ∼1 eV and the monolayer gap can change by as much as ∼6 eV. This establishes the expected need for parameter tuning. Enforcing the IP ansatz, the spread of predicted band gap values is reduced to an insignificant ∼0.1 eV for the bulk, but in the monolayer the spread in band gap values is reduced to a smaller but not negligible ∼0.6 eV, which also affects computed optical spectra. Moreover, there are still many α-γ pairs for bulk or monolayer that satisfy the IP ansatz, and further unequivocal choice of α and γ is needed. Therefore we introduce an additional optimization step, where we plot curves in the α-γ plane that satisfy the IP ansatz of Eq. (3), i.e. $\Delta I = 0$, for *both* bulk and monolayer. The curves, shown in Fig. 1(c), feature a *unique* crossing point, denoted by (α^*, γ^*), which specifies optimal values that are both non-empirical *and* transferable between monolayer and bulk, thereby combining the advantages of WOT-SRSH for 3D solids with SE-SRSH for 2D materials, respectively.

We examine the accuracy of the proposed approach by applying it to bP, MoS_2, and h-BN, in both monolayer and bulk form - see Section II and III of the SI for computational details. First, we examine bP and MoS_2, for which SE-SRSH has already produced accurate band structures and optical absorption spectra, albeit with empirical parameters [44, 45]. We choose MoS_2 because it has been characterized extensively both experimentally and theoretically [1–7, 74–77]. We choose bP because its narrow (∼0.3-0.6 eV), strain-sensitive [23, 78–80] bulk band gap provides a stringent performance test. For MoS_2, the generalized-gradient approximation of Perdew, Burke, and Ernzerhof (PBE)[81] has already proven to be a useful starting point for GW and

TABLE I. GW band gaps based on SE-SRSH ($E_g^{\mathrm{GW@SE}}$) and WOT-SRSH ($E_g^{\mathrm{GW@WOT}}$), as well as SE-SRSH (E_g^{SE}) [44, 45] and WOT-SRSH band gaps (E_g^{WOT}) for the materials studied in this article, compared to computational literature band gaps ($E_g^{\mathrm{lit.}}$). All band gaps are direct, obtained at the Γ point for black phosphorus and at the K point for MoS_2 [61] and h-BN. Numbers in parentheses correspond to calculations with spin-orbit coupling for MoS_2. Numbers in squared parentheses for h-BN correspond to band gaps after subtraction of a ZPR correction (0.26 eV for bulk, 0.38 for 1L).
[A]Ref. 62, value from GW_0. [B]Ref. 63, value from G_0W_0. [C]Refs. 46 and 64, values from G_0W_0. [D]Ref. 65, value from GW_0. [E]Ref. 66, value from G_0W_0. [F]Ref. 67, value from G_0W_0. [G]Ref. 68, value from G_0W_0. [H]Ref. 69, value from eigenvalue-self-consistent GW_0.

Material	Phase	$E_g^{\mathrm{GW@SE}}$ [eV]	$E_g^{\mathrm{GW@WOT}}$ [eV]	E_g^{SE} [eV]	E_g^{WOT} [eV]	$E_g^{\mathrm{lit.}}$ [eV]
bP	Bulk	0.50	0.47	0.56	0.40	0.58[A], 0.3[B]
	1L	2.04	1.98	1.95	1.77	2.00[B] (2.03[C])
MoS_2	Bulk	2.12	2.13	2.03	2.11	(2.00[D])
	1L	2.67 (2.61)	2.54 (2.60)	2.65 (2.55)	2.61 (2.51)	2.47[E], (2.78[F], 2.53[C])
h-BN	Bulk	7.36 [7.10]	7.77 [7.51]	6.63 [6.37]	7.78 [7.52]	6.99[G]
	1L	8.26 [7.88]	8.70 [8.32]	7.26 [6.88]	8.51 [8.13]	8.14[H]

TABLE II. Optical gaps obtained from GW-BSE and TD-SRSH ($E_{\mathrm{opt}}^{\mathrm{GW\text{-}BSE}}$), ($E_{\mathrm{opt}}^{\mathrm{TD\text{-}}}$) based on SE- or WOT-SRSH, compared to literature reference values ($E_{\mathrm{opt}}^{\mathrm{lit.}}$). The optical band gap is dominated by the Γ point for black phosphorus and by the K point for MoS_2 and h-BN. Numbers in parentheses correspond to the position of the first absorption peak upon inclusion of spin-orbit coupling. Numbers in squared parentheses correspond to the position of the peaks upon inclusion of ZPR values (0.26 eV for bulk, 0.38 eV for 1L).
[A]Ref. 63, value from GW-BSE. [B]Ref. 46 and 64, values from GW-BSE. [C]Ref. 65, experimental value. [D]Ref. 70, experimental value. [E]Ref. 71, experimental value. [F]Ref. 69, value from GW-BSE. [G]Ref. 72, experimental value. [H]Ref. 73, experimental value.

Material	Phase	$E_{\mathrm{opt}}^{\mathrm{BSE@SE}}$ [eV]	$E_{\mathrm{opt}}^{\mathrm{BSE@WOT}}$ [eV]	$E_{\mathrm{opt}}^{\mathrm{TD\text{-}SE}}$ [eV]	$E_{\mathrm{opt}}^{\mathrm{TD\text{-}WOT}}$ [eV]	$E_{\mathrm{opt}}^{\mathrm{lit.}}$ [eV]
bP	Bulk	0.39	0.37	0.32	0.26	0.25[A]
	1L	1.44	1.40	1.37	1.28	1.20[A] (1.45[B])
MoS_2	Bulk	1.98	1.99	1.94	1.99	(1.88[C])
	1L	2.09 (A: 2.03, B: 2.20)	2.00 (A: 2.03, B: 2.18)	2.03 (A: 1.94, B: 2.16)	2.06 (A: 1.97, B: 2.18)	2.12[D] (2.07[B])
h-BN	Bulk	6.00 [5.74]	6.25 [5.99]	5.83 [5.57]	6.52 [6.26]	5.99[E]
	1L	5.96 [5.58]	6.22 [5.84]	5.94 [5.56]	6.57 [6.19]	5.95[F], 6.03[G], 6.3[H]

for determining SE-SRSH parameters [44]. It is therefore used here as well to calculate the dielectric constant in the initial step of the WOT-SRSH procedure. For bP, owing to the narrow bulk band gap, PBE is known to erroneously predict a metallic ground state [82–84] and in this case we use the short-range hybrid functional of Heyd, Scuseria, and Ernzerhof (HSE)[85, 86] instead of PBE [45].

Using the above-described procedure, we obtain optimal (α^*, γ^*) pairs of (0.152, 0.027Å^{-1}) and (0.126, 0.030Å^{-1}) for bP and MoS_2, respectively (see Section II of the SI for detailed parameters). These values differ (by 12-16% for α^* and 24-26% for γ^*) from those obtained with the semiempirical procedure (see SI),[44, 45] which is expected given that the IP ansatz is satisfied in one case (WOT-SRSH) whereas target band gaps are fitted in the other (SE-SRSH). The band structures obtained from each method are compared in Figs. 2(a-b) and 3(a-b) for bP and MoS_2, respectively. Remarkably, despite their different parameters, WOT-SRSH and SE-SRSH produce bandstructures that are in strikingly good agreement. As the SE-SRSH band structures were already shown to be in excellent agreement with GW calculations [44, 45], so too are our WOT-SRSH results. Quantitatively, corresponding fundamental band gaps, also compared to literature values, are given in Table I. Once again, the SE- and WOT-SRSH values agree very well with each other (maximum deviation of ∼0.18 eV, for bulk MoS_2). Even more importantly, Table I shows that our results compare very well with reference literature data, i.e., are within the range of reported band gaps. This establishes the predictive power of our approach for fundamental band gaps and band structures.

The calculation of accurate optical absorption spectra presents an even more stringent test for the predictive capacity of the SRSH functionals, as a correct description of exciton (de-)localization is needed. Results obtained from time-dependent SRSH (TD-SE-SRSH/TD-WOT-SRSH) calculations for bulk and monolayer bP and MoS_2 are given in Figs. 2(c-d) and 3(c-d), respectively. Clearly, the spectral lineshapes obtained with either approach, for both bulk and monolayer are essentially the same, with very small shifts between the two spectra (maximal shift of ∼ 0.15 eV, for monolayer bP). Further-

more, optical gaps, reported in Table II, are in excellent agreement with literature values. The Table also shows that for the MoS_2 monolayer we can accurately resolve the A and B spin-orbit split exciton peaks.

To examine further the accuracy of the SRSH functionals, we perform full-frequency, single-shot, G_0W_0 (henceforth, "GW") calculations,[87] starting from the SE-/WOT-SRSH wavefunctions and eigenenergies, followed by BSE calculations for optical absorption spectra. The results are also shown in Figs. 2 (c-d) and 3(c-d), with fundamental (GW) and optical (GW-BSE) gaps reported in Tables I and II; the dashed vertical lines in the figures indicate the calculated direct GW quasiparticle gaps. Importantly, the line-shapes obtained from TDDFT and from GW-BSE are essentially identical and quantitative shifts between the spectra obtained from either methods are within the typical accuracy of either calculation, i.e., 0.1-0.2 eV. The fact that GW corrections to WOT-SRSH change the band gap for bulk by $\sim$0.2 eV at most, and usually less (as found previously for non-layered materials [39, 40]), reflects the quantitative accuracy of the WOT-SRSH approach. Thus, WOT-SRSH is shown to be equally useful in itself or as an optimal starting point for *ab initio* many-body perturbation theory [39, 40].

We now turn to h-BN, a wide-gap semiconductor. Particularly in monolayer form, it has proven challenging to predict accurately from first principles in general [88] and using SE-SRSH in particular [44]. Recent work has reported that obtaining accurate quasiparticle gaps (and subsequent absorption spectra) for monolayer h-BN requires eigenvalue-self-consistent GW_0 calculations for a semilocal functional starting point.[69] We therefore examine whether the WOT-SRSH method can overcome these challenges.

Figure 4(a,b) displays optical absorption spectra for bulk and monolayer h-BN, obtained from TD-SE- and TD-WOT-SRSH calculations, as well as from GW-BSE calculations based on SE-/WOT-SRSH ground states as a starting point. Corresponding fundamental and optical band gaps are reported in Tables I and II, respectively. In agreement with Ref. [44], we find that the TD-SE-SRSH absorption spectra suffer from both qualitative and quantitative shortcomings, in the form of spurious satellite peaks and incorrect absorption onsets, respectively. These deficiencies are ameliorated by performing a GW calculation based on the SE-SRSH ground state and naively one could deduce that at least for the bulk (Figure 4), quantitative agreement with experiment is obtained, an issue we return to below. Importantly, spectra based on WOT-SRSH do not show a spurious line-shape even in the absence of GW-BSE corrections, thereby resolving a significant disadvantage of SE-SRSH while removing empiricism. And once again, spectral shifts upon application of GW-BSE from a WOT-SRSH starting point are small and the lineshapes are essentially the same.

Here, we note that electron-phonon interactions [89, 90] can lead to significant ZPR of electronic band gaps in materials with light elements, such as the B and N atoms found in h-BN [88, 91, 92]. To account for this, we compute ZPR corrections to the fundamental gap of both bulk and monolayer h-BN using a finite difference approach [93–95] (see Sections I and II of the SI for details). We obtain ZPR shifts of 0.26 eV and 0.38 eV for the bulk and monolayer, respectively. Computed optical spectra that are shifted by these ZPR values are given in Figure 4(c,d). For bulk h-BN, inclusion of the ZPR worsens the agreement between the GW-BSE@SE-SRSH absorption spectrum and experiment, indicating a partly fortuitous agreement in the absence of ZPR. For monolayer h-BN, GW-BSE@SE-SRSH calculations improves the spectral lineshape with respect to SE-SRSH, but does not fully address disagreement with experiment, which is already evident without ZPR corrections and only worsens upon inclusion of the latter. In contrast, results based on the WOT-SRSH functional show improvement upon inclusion of the ZPR.

The above discussion immediately clarifies the origins of the limitations of the SE-SRSH functional for h-BN [44], as well as why it is apparent only in this large gap material. The SE-SRSH was fit to a significantly underestimated fundamental gap (7.26 eV at the K point) because GW with a local density approximation (LDA) starting point was used, whereas the WOT-SRSH band gap is substantially larger (8.13 eV at the K point), consistent with self-consistent GW results [69]. This underestimate by SE-SRSH and GW-BSE@PBE was partly offset by the neglect of ZPR, but errors remained. With WOT-SRSH, in contrast, the pertinent physical effects (single-particle excitations, exciton formation, phonon renormalization) are all accounted for systematically.

In conclusion, we have presented a non-empirical and internally self-consistent approach to designing screened range-separated hybrid functionals that can deliver quantitatively accurate predictions of electronic and optical properties of layered van der Waals materials. These functionals already rival more expensive state-of-the-art methods such as GW-BSE at reduced computational cost and, moreover, if so desired can provide excellent starting points for higher-levels of theory. In particular, the straightforward resolution of the inaccuracies in quasiparticle and optical gaps for h-BN demonstrates the robustness of this approach and highlights its potential for modeling a broad range of 2D/layered semiconductors and insulators.

ACKNOWLEDGMENTS

We thank Prof. Bartomeu Monserrat for very helpful input regarding the effects of ZPR and Dr. Daniel Hernangómez-Pérez for useful discussions. This work was supported by the U.S.-Israel NSF–Binational Science Foundation Grant No. DMR-2015991, by the US Air Force through the grant AFOSR grant FA8655-20-1-7041, and by the Israel Science Foundation. M.C.-G.

is grateful to the Azrieli Foundation for the award of an Azrieli International Postdoctoral Fellowship. This work used Frontera at TACC in part through allocation TG-DMR190070 from the Extreme Science and Engineering Discovery Environment (XSEDE) [96], which was supported by National Science Foundation grant number #1548562 and the Advanced Cyberinfrastructure Coordination Ecosystem: Services & Support (ACCESS) program, which is supported by National Science Foundation grants #2138259, #2138286, #2138307, #2137603, and #2138296. Additional computational resources were provided by the Weizmann Institute of Science at Chemfarm. L.K. acknowledges support from the Aryeh and Mintzi Katzman Professorial Chair, and the Helen and Martin Kimmel Award for Innovative Investigation. A.R. gratefully acknowledges support from the National Science Foundation (NSF-BSF 2150562).

[1] K. S. Novoselov, A. K. Geim, S. V. Morozov, D. Jiang, Y. Zhang, S. V. Dubonos, I. V. Grigorieva, and A. A. Firsov, Electric field effect in atomically thin carbon films, Science **306**, 666 (2004).
[2] K. S. Novoselov, D. Jiang, F. Schedin, T. J. Booth, V. V. Khotkevich, S. V. Morozov, and A. K. Geim, Two-dimensional atomic crystals, PNAS **102**, 10451 (2005).
[3] Q. H. Wang, K. Kalantar-Zadeh, A. Kis, J. N. Coleman, and M. S. Strano, Electronics and optoelectronics of two-dimensional transition metal dichalcogenides, Nature Nanotech. **7**, 699 (2012).
[4] A. K. Geim and I. V. Grigorieva, Van der Waals heterostructures, Nature **499**, 419 (2013).
[5] Y. Liu, N. O. Weiss, X. Duan, H.-C. Cheng, Y. Huang, and X. Duan, Van der Waals heterostructures and devices, Nat. Rev. Mater. **1**, 16042 (2016).
[6] K. S. Novoselov, A. Mishchenko, A. Carvalho, and A. H. C. Neto, 2D materials and van der Waals heterostructures, Science **353**, aac9439 (2016).
[7] P. M. Ajayan, P. Kim, and K. Banerjee, Two-dimensional van der Waals materials, Phys. Today **69**, 38 (2016).
[8] M. Bernardi, C. Ataca, M. Palummo, and J. C. Grossman, Optical and electronic properties of two-dimensional layered materials, Nanophotonics **6**, 479 (2017).
[9] A. Yadav, C. M. Acosta, G. M. Dalpian, and O. I. Malyi, First-principles investigations of 2D materials: Challenges and best practices, Matter **6**, 2711 (2023).
[10] L. Hedin, New method for calculating the one-particle Green's function with application to the electron-gas problem, Phys. Rev. **139**, A796 (1965).
[11] G. Onida, L. Reining, and A. Rubio, Electronic excitations: density-functional versus many-body Green's-function approaches, Rev. Mod. Phys. **74**, 601 (2002).
[12] M. S. Hybertsen and S. G. Louie, Electron correlation in semiconductors and insulators: Band gaps and quasiparticle energies, Phys. Rev. B **34**, 5390 (1986).
[13] M. Rohlfing and S. G. Louie, Electron-hole excitations in semiconductors and insulators, Phys. Rev. Lett. **81**, 2312 (1998).
[14] S. Albrecht, L. Reining, R. Del Sole, and G. Onida, Ab initio calculation of excitonic effects in the optical spectra of semiconductors, Phys. Rev. Lett. **80**, 4510 (1998).
[15] R. G. Parr and W. Yang, Density Functional Theory of Atoms and Molecules (Oxford University Press, Oxford, 1989).
[16] M. Dreizler and E. K. U. Gross, Density Functional Theory: An Approach to the Quantum Many-Body Problem (Springer, Berlin, 1990).
[17] J. Ma and L.-W. Wang, Using Wannier functions to improve solid band gap predictions in density functional theory, Sci. Rep. **6**, 24924 (2016).
[18] M. Weng, S. Li, J. Ma, J. Zheng, F. Pan, and L.-W. Wang, Wannier Koopman method calculations of the band gaps of alkali halides, Appl. Phys. Lett. **111**, 054101 (2017).
[19] N. L. Nguyen, N. Colonna, A. Ferretti, and N. Marzari, Koopmans-compliant spectral functionals for extended systems, Phys. Rev. X **8**, 021051 (2018).
[20] N. Colonna, N. L. Nguyen, A. Ferretti, and N. Marzari, Koopmans-compliant functionals and potentials and their application to the GW100 test set, J. Chem. Theory Comput. **15**, 1905 (2019).
[21] N. Colonna, R. De Gennaro, E. Linscott, and N. Marzari, Koopmans spectral functionals in periodic boundary conditions, J. Chem. Theory Comput. **18**, 5435 (2022).
[22] E. B. Linscott, N. Colonna, R. De Gennaro, N. L. Nguyen, G. Borghi, A. Ferretti, I. Dabo, and N. Marzari, koopmans: An open-source package for accurately and efficiently predicting spectral properties with koopmans functionals, J. Chem. Theory Comput. **19**, 7097 (2023).
[23] X. Li, J. Sun, P. Shahi, M. Gao, A. H. MacDonald, Y. Uwatoko, T. Xiang, J. B. Goodenough, J. Cheng, and J. Zhou, Pressure-induced phase transitions and superconductivity in a black phosphorus single crystal, PNAS **115**, 9935 (2018).
[24] Y. Mei, Z. Chen, and W. Yang, Self-consistent calculation of the localized orbital scaling correction for correct electron densities and energy-level alignments in density functional theory, J. Phys. Chem. Lett. **11**, 10269 (2020).
[25] A. Mahler, J. Williams, N. Q. Su, and W. Yang, Localized orbital scaling correction for periodic systems, Phys. Rev. B **106**, 035147 (2022).
[26] T. Shimazaki and Y. Asai, First principles band structure calculations based on self-consistent screened Hartree–Fock exchange potential, J. Chem. Phys. **130**, 164702 (2009).
[27] J. H. Skone, M. Govoni, and G. Galli, Self-consistent hybrid functional for condensed systems, Phys. Rev. B **89**, 195112 (2014).
[28] J. H. Skone, M. Govoni, and G. Galli, Nonempirical range-separated hybrid functionals for solids and molecules, Phys. Rev. B **93**, 235106 (2016).
[29] W. Chen, G. Miceli, G.-M. Rignanese, and A. Pasquarello, Nonempirical dielectric-dependent hybrid functional with range separation for semiconductors and insulators, Phys. Rev. Mater. **2**, 073803 (2018).
[30] J. Sun, J. Yang, and C. A. Ullrich, Low-cost alternatives to the Bethe-Salpeter equation: Towards simple hybrid

functionals for excitonic effects in solids, Phys. Rev. Res. **2**, 013091 (2020).
[31] J. Zhan, M. Govoni, and G. Galli, Nonempirical range-separated hybrid functional with spatially dependent screened exchange, J. Chem. Theory Comput. **19**, 5851 (2023).
[32] S. Refaely-Abramson, S. Sharifzadeh, M. Jain, R. Baer, J. B. Neaton, and L. Kronik, Gap renormalization of molecular crystals from density-functional theory, Phys. Rev. B **88**, 081204 (2013).
[33] S. Refaely-Abramson, M. Jain, S. Sharifzadeh, J. B. Neaton, and L. Kronik, Solid-state optical absorption from optimally tuned time-dependent range-separated hybrid density functional theory, Phys. Rev. B **92**, 081204 (2015).
[34] G. Miceli, W. Chen, I. Reshetnyak, and A. Pasquarello, Nonempirical hybrid functionals for band gaps and polaronic distortions in solids, Phys. Rev. B **97**, 121112 (2018).
[35] T. Bischoff, I. Reshetnyak, and A. Pasquarello, Adjustable potential probes for band-gap predictions of extended systems through nonempirical hybrid functionals, Phys. Rev. B **99**, 201114 (2019).
[36] J. Yang, S. Falletta, and A. Pasquarello, Range-separated hybrid functionals for accurate prediction of band gaps of extended systems, NPJ Comp. Mater. **9**, 108 (2023).
[37] D. Wing, G. Ohad, J. B. Haber, M. R. Filip, S. E. Gant, J. B. Neaton, and L. Kronik, Band gaps of crystalline solids from Wannier-localization based optimal tuning of a screened range-separated hybrid functional, PNAS **118**, e2104556118 (2021).
[38] G. Ohad, D. Wing, S. E. Gant, A. V. Cohen, J. B. Haber, F. Sagredo, M. R. Filip, J. B. Neaton, and L. Kronik, Band gaps of halide perovskites from a Wannier-localized optimally tuned screened range-separated hybrid functional, Phys. Rev. Materials **6**, 104606 (2022).
[39] S. E. Gant, J. B. Haber, M. R. Filip, F. Sagredo, D. Wing, G. Ohad, L. Kronik, and J. B. Neaton, Optimally tuned starting point for single-shot GW calculations of solids, Phys. Rev. Mater. **6**, 053802 (2022).
[40] G. Ohad, S. E. Gant, D. Wing, J. B. Haber, M. Camarasa-Gómez, F. Sagredo, M. R. Filip, J. B. Neaton, and L. Kronik, Optical absorption spectra of metal oxides from time-dependent density functional theory and many-body perturbation theory based on optimally-tuned hybrid functionals, Phys. Rev. Mater. **7**, 123803 (2023).
[41] G. Ohad, M. Hartstein, T. Gould, J. B. Neaton, and L. Kronik, Non-empirical prediction of the length-dependent ionization potential in molecular chains (2024), arXiv:2403.18518 [physics.chem-ph].
[42] L. Kronik and J. B. Neaton, Excited-state properties of molecular solids from first principles, Annu. Rev. Phys. Chem. **67**, 587 (2016).
[43] L. Kronik and S. Kümmel, Dielectric screening meets optimally tuned density functionals, Adv. Mater. **30**, 1706560 (2018).
[44] A. Ramasubramaniam, D. Wing, and L. Kronik, Transferable screened range-separated hybrids for layered materials: The cases of MoS_2 and h-BN, Phys. Rev. Materials **3**, 084007 (2019).
[45] M. Camarasa-Gómez, A. Ramasubramaniam, J. B. Neaton, and L. Kronik, Transferable screened range-separated hybrid functionals for electronic and optical properties of van der waals materials, Phys. Rev. Mater. **7**, 104001 (2023).
[46] S. Haastrup, M. Strange, M. Pandey, T. Deilmann, P. S. Schmidt, N. F. Hinsche, M. N. Gjerding, D. Torelli, P. M. Larsen, A. C. Riis-Jensen, J. Gath, K. W. Jacobsen, J. J. Mortensen, T. Olsen, and K. S. Thygesen, The computational 2D materials database: high-throughput modeling and discovery of atomically thin crystals, 2D Materials **5**, 042002 (2018).
[47] X. Zhang, A. Chen, and Z. Zhou, High-throughput computational screening of layered and two-dimensional materials, WIREs Comp. Mol. Sci. **9**, e1385 (2019).
[48] T. Leininger, H. Stoll, H.-J. Werner, and A. Savin, Combining long-range configuration interaction with short-range density functionals, Chem. Phys. Lett. **275**, 151 (1997).
[49] T. Yanai, D. P. Tew, and N. C. Handy, A new hybrid exchange–correlation functional using the Coulomb-attenuating method (CAM-B3LYP), Chem. Phys. Lett. **393**, 51 (2004).
[50] D. Wing, J. B. Haber, R. Noff, B. Barker, D. A. Egger, A. Ramasubramaniam, S. G. Louie, J. B. Neaton, and L. Kronik, Comparing time-dependent density functional theory with many-body perturbation theory for semiconductors: Screened range-separated hybrids and the GW plus Bethe-Salpeter approach, Phys. Rev. Materials **3**, 064603 (2019).
[51] A. Seidl, A. Görling, P. Vogl, J. A. Majewski, and M. Levy, Generalized Kohn-Sham schemes and the band-gap problem, Phys. Rev. B **53**, 3764 (1996).
[52] S. Kümmel and L. Kronik, Orbital-dependent density functionals: Theory and applications, Rev. Mod. Phys. **80**, 3 (2008).
[53] L. Kronik, T. Stein, S. Refaely-Abramson, and R. Baer, Excitation Gaps of Finite-Sized Systems from Optimally Tuned Range-Separated Hybrid Functionals, J. Chem. Theory Comput. **8**, 1515 (2012).
[54] J. P. Perdew, W. Yang, K. Burke, Z. Yang, E. K. U. Gross, M. Scheffler, G. E. Scuseria, T. M. Henderson, I. Y. Zhang, A. Ruzsinszky, H. Peng, J. Sun, E. Trushin, and A. Görling, Understanding band gaps of solids in generalized Kohn–Sham theory, PNAS **114**, 2801 (2017).
[55] R. Baer and L. Kronik, Time-dependent generalized Kohn–Sham theory, Eur. Phys. J. B **91**, 170 (2019).
[56] P. Cudazzo, I. V. Tokatly, and A. Rubio, Dielectric screening in two-dimensional insulators: Implications for excitonic and impurity states in graphane, Phys. Rev. B **84**, 085406 (2011).
[57] K. Andersen, S. Latini, and K. S. Thygesen, Dielectric genome of van der Waals heterostructures, Nano Lett. **15**, 4616 (2015).
[58] D. Y. Qiu, F. H. da Jornada, and S. G. Louie, Screening and many-body effects in two-dimensional crystals: Monolayer MoS_2, Phys. Rev. B **93**, 235435 (2016).
[59] R. W. Nunes and X. Gonze, Berry-phase treatment of the homogeneous electric field perturbation in insulators, Phys. Rev. B **63**, 155107 (2001).
[60] I. Souza, J. Íñiguez, and D. Vanderbilt, First-principles approach to insulators in finite electric fields, Phys. Rev. Lett. **89**, 117602 (2002).
[61] The smallest gap for the monolayer is indirect, between Γ and K, rather than direct at K due to a biaxial tensile strain of ∼1.15% that arises from using the experimental lattice parameter. This has no bearing on the overall

conclusions of this paper.

[62] V. Wang, Y. Kawazoe, and W. T. Geng, Native point defects in few-layer phosphorene, Phys. Rev. B **91**, 045433 (2015).

[63] V. Tran, R. Soklaski, Y. Liang, and L. Yang, Layer-controlled band gap and anisotropic excitons in few-layer black phosphorus, Phys. Rev. B **89**, 235319 (2014).

[64] M. N. Gjerding, A. Taghizadeh, A. Rasmussen, S. Ali, F. Bertoldo, T. Deilmann, N. R. Knøsgaard, M. Kruse, A. H. Larsen, S. Manti, T. G. Pedersen, U. Petralanda, T. Skovhus, M. K. Svendsen, J. J. Mortensen, T. Olsen, and K. S. Thygesen, Recent progress of the computational 2D materials database (c2db), 2D Materials **8**, 044002 (2021).

[65] H.-P. Komsa and A. V. Krasheninnikov, Effects of confinement and environment on the electronic structure and exciton binding energy of mos_2 from first principles, Phys. Rev. B **86**, 241201 (2012).

[66] M. Graml, K. Zollner, D. Hernangómez-Pérez, P. E. Faria Junior, and J. Wilhelm, Low-scaling GW algorithm applied to twisted transition-metal dichalcogenide heterobilayers, J. Chem. Theory Comp. **20**, 2202 (2024).

[67] D. Y. Qiu, F. H. da Jornada, and S. G. Louie, Optical spectrum of mos_2: Many-body effects and diversity of exciton states, Phys. Rev. Lett. **111**, 216805 (2013).

[68] M. Kolos and F. Karlický, Accurate many-body calculation of electronic and optical band gap of bulk hexagonal boron nitride, Phys. Chem. Chem. Phys. **21**, 3999 (2019).

[69] F. Zhang, C. S. Ong, J. W. Ruan, M. Wu, X. Q. Shi, Z. K. Tang, and S. G. Louie, Intervalley excitonic hybridization, optical selection rules, and imperfect circular dichroism in monolayer $h-$BN, Phys. Rev. Lett. **128**, 047402 (2022).

[70] B. Zhu, X. Chen, and X. Cui, Exciton binding energy of monolayer WS_2, Sci. Rep. **5**, 9218 (2015).

[71] C. Tarrio and S. E. Schnatterly, Interband transitions, plasmons, and dispersion in hexagonal boron nitride, Phys. Rev. B **40**, 7852 (1989).

[72] X. Li, H. Qiu, X. Liu, J. Yin, and W. Guo, Wettability of supported monolayer hexagonal boron nitride in air, Adv. Funct. Mater. **27**, 1603181 (2017).

[73] R. J. P. Román Peña, F. J. R. Costa Costa, A. Zobelli, C. Elias, P. Valvin, G. Cassabois, B. Gil, A. Summerfield, T. S. Cheng, C. J. Mellor, P. H. Beton, S. V. Novikov, and L. Z. Zagonel, Band gap measurements of monolayer h-BN and insights into carbon-related point defects, 2D Materials **8**, 044001 (2021).

[74] B. Radisavljevic, A. Radenovic, J. Brivio, V. Giacometti, and A. Kis, Single-layer MoS_2 transistors, Nature Nanotechnology **6**, 147 (2011).

[75] O. Lopez-Sanchez, D. Lembke, M. Kayci, A. Radenovic, and A. Kis, Ultrasensitive photodetectors based on monolayer MoS_2, Nature Nanotechnology **8**, 497 (2013).

[76] D. Jariwala, V. K. Sangwan, L. J. Lauhon, T. J. Marks, and M. C. Hersam, Emerging device applications for semiconducting two-dimensional transition metal dichalcogenides, ACS Nano **8**, 1102 (2014).

[77] E. Y. Andrei, D. K. Efetov, P. Jarillo-Herrero, A. H. MacDonald, K. F. Mak, T. Senthil, E. Tutuc, A. Yazdani, and A. F. Young, The marvels of Moiré materials, Nat. Rev. Mater. **6**, 201 (2021).

[78] X. Ling, H. Wang, S. Huang, F. Xia, and M. S. Dresselhaus, The renaissance of black phosphorus, PNAS **112**, 4523 (2015).

[79] Y. Xu, Z. Shi, X. Shi, K. Zhang, and H. Zhang, Recent progress in black phosphorus and black-phosphorus-analogue materials: properties, synthesis and applications, Nanoscale **11**, 14491 (2019).

[80] J. Cheng, L. Gao, T. Li, S. Mei, C. Wang, B. Wen, W. Huang, C. Li, G. Zheng, H. Wang, and H. Zhang, Two-dimensional black phosphorus nanomaterials: Emerging advances in electrochemical energy storage science, Nanomicro Lett. **12**, 179 (2020).

[81] J. P. Perdew, K. Burke, and M. Ernzerhof, Generalized Gradient Approximation Made Simple, Phys. Rev. Lett. **77**, 3865 (1996).

[82] T. Kotani and M. van Schilfgaarde, All-electron GW approximation with the mixed basis expansion based on the full-potential LMTO method, Solid State Commun. **121**, 461 (2002).

[83] M. van Schilfgaarde, T. Kotani, and S. V. Faleev, Adequacy of approximations in GW theory, Phys. Rev. B **74**, 245125 (2006).

[84] F. Fuchs, J. Furthmüller, F. Bechstedt, M. Shishkin, and G. Kresse, Quasiparticle band structure based on a generalized Kohn-Sham scheme, Phys. Rev. B **76**, 115109 (2007).

[85] J. Heyd, G. E. Scuseria, and M. Ernzerhof, Hybrid functionals based on a screened Coulomb potential, J. Chem. Phys. **118**, 8207 (2003).

[86] J. Heyd, G. E. Scuseria, and M. Ernzerhof, Erratum: "Hybrid functionals based on a screened Coulomb potential" [J. Chem. Phys. 118, 8207 (2003)], J. Chem. Phys. **124**, 219906 (2006).

[87] M. Shishkin and G. Kresse, Implementation and performance of the frequency-dependent GW method within the PAW framework, Phys. Rev. B **74**, 035101 (2006).

[88] R. J. Hunt, B. Monserrat, V. Zólyomi, and N. D. Drummond, Diffusion quantum Monte Carlo and *GW* study of the electronic properties of monolayer and bulk hexagonal boron nitride, Phys. Rev. B **101**, 205115 (2020).

[89] P. B. Allen and V. Heine, Theory of the temperature dependence of electronic band structures, J. Phys. C: Solid State Phys. **9**, 2305 (1976).

[90] P. B. Allen and M. Cardona, Theory of the temperature dependence of the direct gap of germanium, Phys. Rev. B **23**, 1495 (1981).

[91] R. Tutchton, C. Marchbanks, and Z. Wu, Structural impact on the eigenenergy renormalization for carbon and silicon allotropes and boron nitride polymorphs, Phys. Rev. B **97**, 205104 (2018).

[92] H. Mishra and S. Bhattacharya, Giant exciton-phonon coupling and zero-point renormalization in hexagonal monolayer boron nitride, Phys. Rev. B **99**, 165201 (2019).

[93] J. H. Lloyd-Williams and B. Monserrat, Lattice dynamics and electron-phonon coupling calculations using nondiagonal supercells, Phys. Rev. B **92**, 184301 (2015).

[94] B. Monserrat, Correlation effects on electron-phonon coupling in semiconductors: Many-body theory along thermal lines, Phys. Rev. B **93**, 100301 (2016).

[95] B. Monserrat, Electron–phonon coupling from finite differences, J. Phys.: Condens. Matter **30**, 083001 (2018).

[96] J. Towns, T. Cockerill, M. Dahan, I. Foster, K. Gaither, A. Grimshaw, V. Hazlewood, S. Lathrop, D. Lifka, G. D. Peterson, R. Roskies, J. R. Scott, and N. Wilkins-Diehr, XSEDE: Accelerating scientific discovery, Comput. Sci. Eng. **16**, 62 (2014).

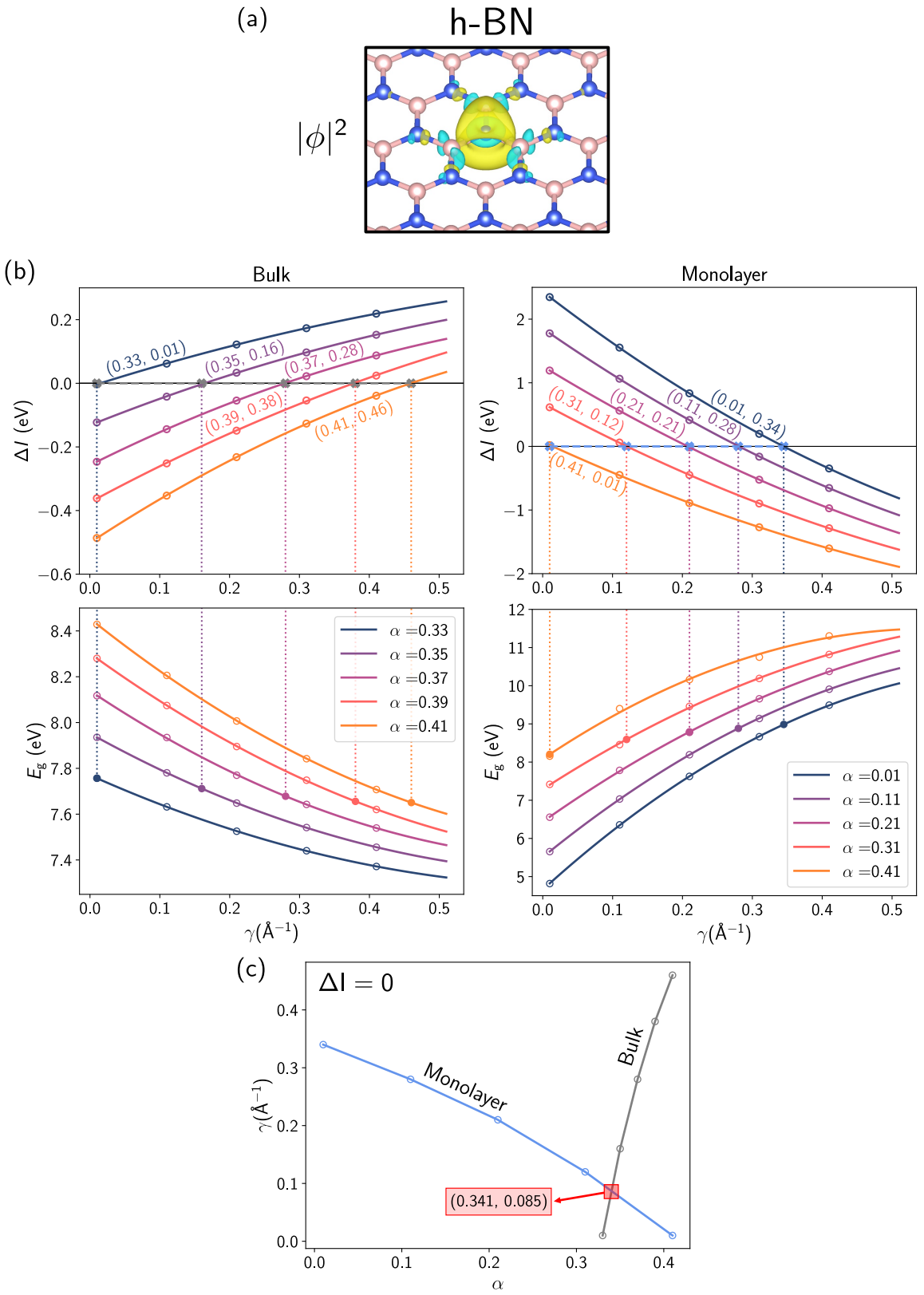

FIG. 1. Demonstration of the non-empirical WOT-SRSH method, as applied to h-BN: (a) highest-expectation-value occupied maximally-localized Wannier function; (b) The IP ansatz target function, ΔI (top) and the fundamental band gap, E_g, at the K-point (bottom), for both bulk (ϵ_∞ of the solid, left) and monolayer ($\epsilon_\infty = 1$, right), as a function of the range-separation parameter, γ, for different values of the fraction of short-range exact exchange, α. Circles indicated computed data points and the lines are a guide to the eye. Closed circles have been obtained from (α, γ) pairs that obey the IP ansatz, with the parameter values shown; (c) IP ansatz fulfillment ($\Delta I = 0$) curves in the (α, γ) plane for monolayer and bulk, with their point of intersection, (α^*, γ^*), obeying the IP ansatz for both phases simultaneously and used for predictive calculations.

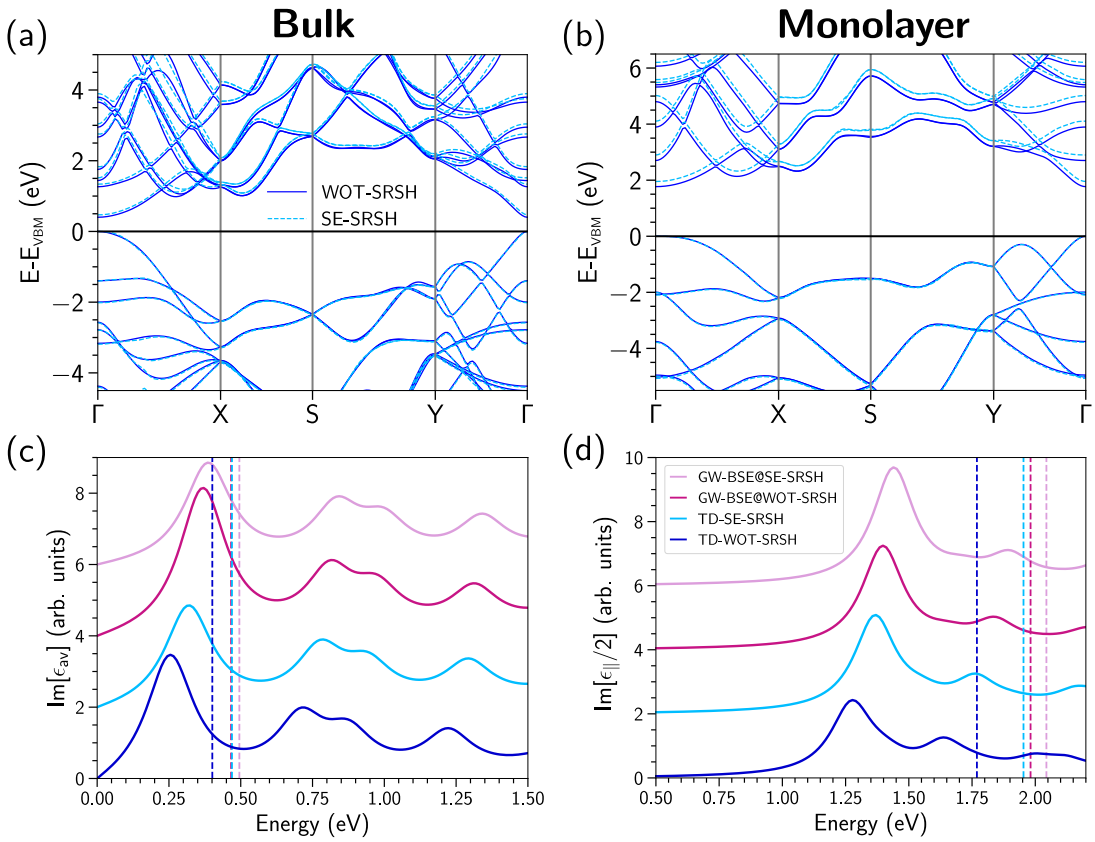

FIG. 2. (a), (b) Bandstructures of bulk and monolayer black phosphorus, calculated using SE- and WOT-SRSH functionals. (c), (d) Optical absorption spectra for bulk and monolayer black phosphorus, obtained from TD-SE-SRSH and TD-WOT-SRSH, as well as from "single-shot" GW-BSE using SE- and WOT-SRSH as starting points. Dashed vertical lines represent the fundamental band gap. SE-SRSH data are taken from Ref. [45].

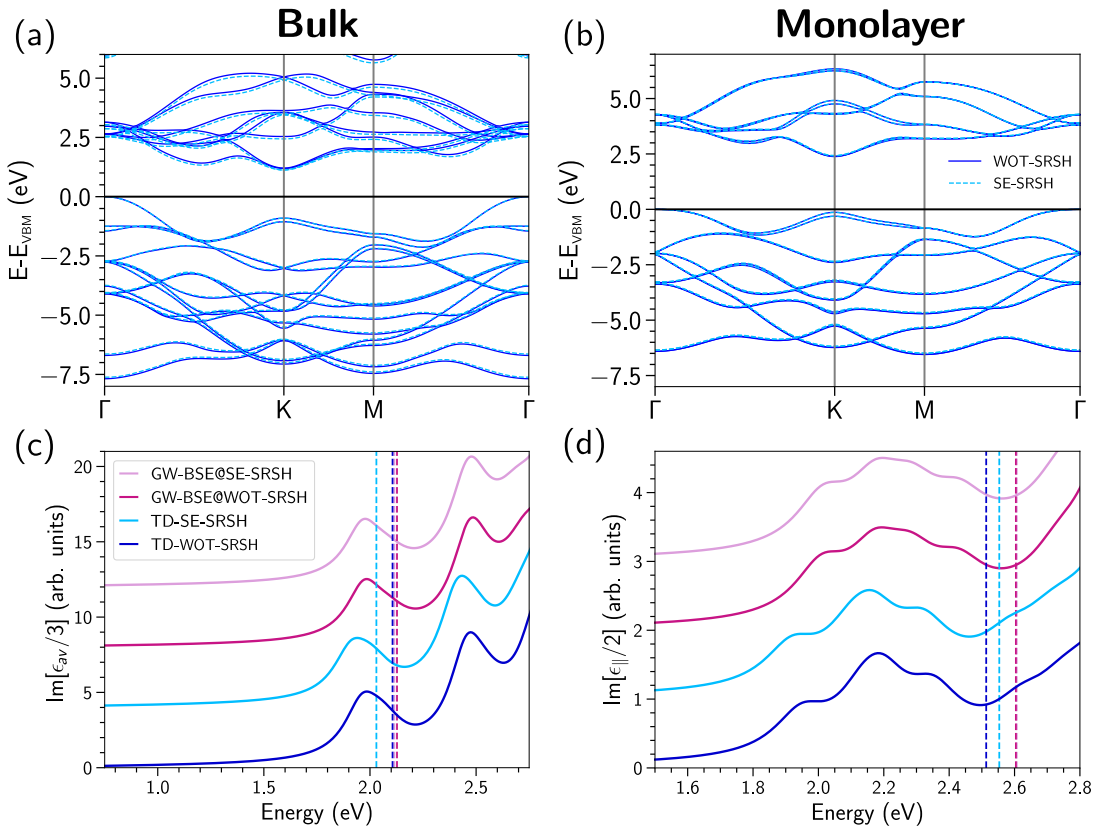

FIG. 3. (a), (b) Bandstructures of bulk and monolayer MoS_2, calculated using SE- and WOT-SRSH functionals [61]. (c), (d) Optical absorption spectra for bulk and monolayer MoS_2, obtained from TD-SE-SRSH and TD-WOT-SRSH, as well as from "single-shot" GW-BSE using SE- and WOT-SRSH as starting points. Dashed vertical lines represent the fundamental band gap. SE-SRSH data are taken from Ref. [45]. All monolayer calculations include spin-orbit coupling.

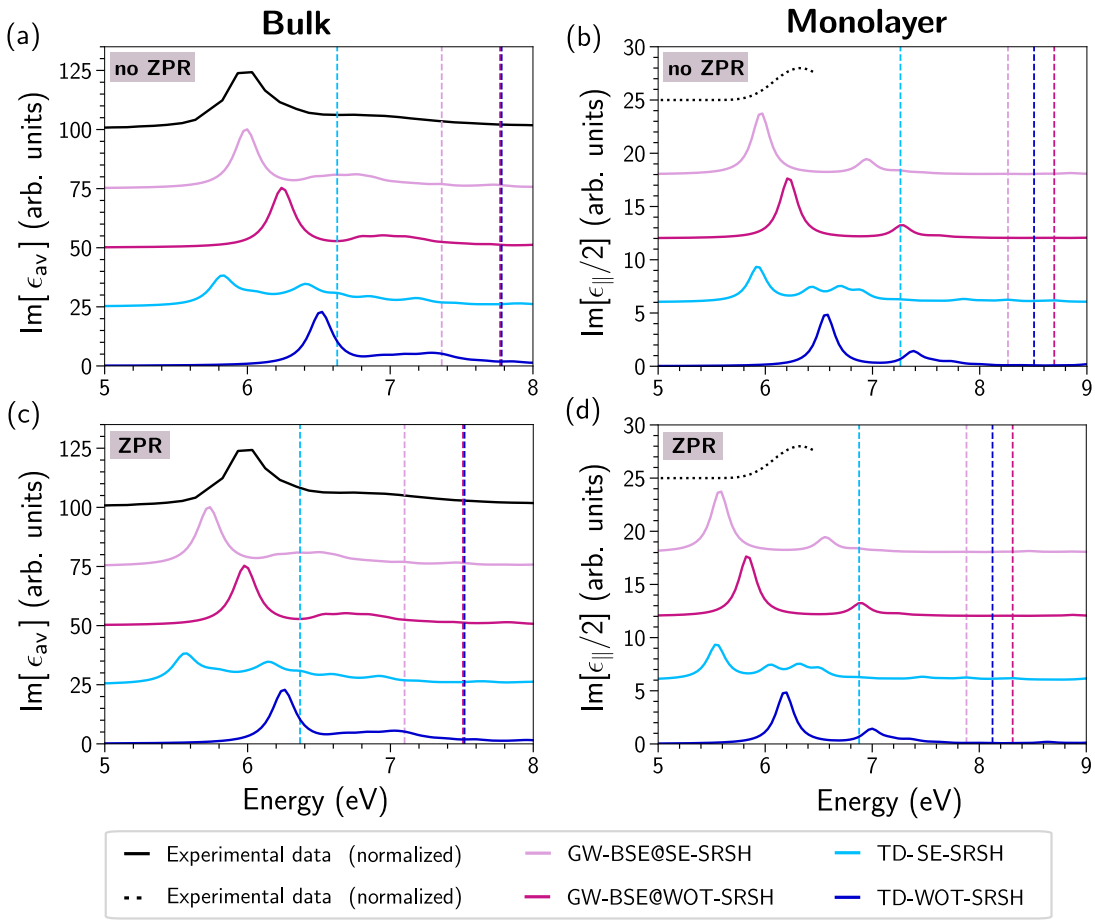

FIG. 4. Optical absorption spectra for (a, b) bulk and (c, d) monolayer h-BN. Experimental absorption spectra are extracted from Ref. [71] for bulk h-BN and from Ref. [73] for the monolayer. Dashed vertical lines represent the fundamental band gap. (a, c) and (b, d) show results without and with subtraction of ZPR corrections, respectively.